RSC Advances

PAPER

View Article Online
View Journal | View Issue

Cite this: *RSC Adv.*, 2015, **5**, 63215

Novel quaternary ammonium functional addition-type norbornene copolymer as hydroxide-conductive and durable anion exchange membrane for direct methanol fuel cells

Xiaohui He,*[ab] Jingyin Liu,[ab] Hongyu Zhu,[a] Yan Zheng[a] and Defu Chen[c]

Received 19th May 2015
Accepted 16th July 2015

DOI: 10.1039/c5ra09393g

www.rsc.org/advances

Novel quaternary ammonium functional addition-type norbornene copolymers (Q_{Cn}P(BN/PhBN), $n = 1$, 6, 10, 12) with different alkyl side chain length comb-shaped structures or different contents of 2-(4-phenyl-butoxymethy-lene)-5-norbornene (PhBN) (22–77%) are synthesized *via* copolymerization of functionalized norbornenes, and their corresponding hydroxide-conductive anion exchange membranes (AEMs) with effective hydrophilic–hydrophobic separation are prepared and confirmed by TEM or SEM. The achieved AEMs show high ion exchange capacity (1.83 mmol g^{-1}), as well as low methanol permeability (1.97–20.4 $\times$ 10^{-7} cm^2 s^{-1}), which are lower than that of Nafion®. The ionic conductivity increases with the operation temperature increasing and is observed up to 4.14 $\times$ 10^{-3} S cm^{-1}. The AEMs exhibit excellent dimensional stability with a swelling degree in plane between 0.9–3.3% and good chemical stability under 6 M NaOH solution even after a month. Membrane electrode assembly (MEA) is fabricated by using the alkalized Q_{C12}P(BN/PhBN)-77 as the AEM and tested in an alkaline direct methanol fuel cell. The open circuit voltage (OVC) of 0.54 V and the maximum current density of 66 mW cm^{-2} are achieved at 80 °C, respectively.

1 Introduction

Fuel cells are efficient energy conversion devices that can directly convert chemical energy to electricity and have been attracting attention as a clean energy technology.[1,2] They are mainly divided into proton exchange membrane direct methanol fuel cells (PEMDMFC) and anion exchange membrane direct methanol fuel cells (AEMDMFC). The most widespread fuel cell technologies are based on the proton-exchange membrane fuel cell (PEMFC). Nafion, produced by DuPont, is the preferred polymer electrolyte membrane in the PEMFC, which is a perfiuorosulfonated copolymer that exhibits high ionic conductivity and dimensional stability. Nevertheless, PEMFCs must use platinum as the catalyst or other precious metal-based catalysts, and have limited lifetime for easy degradation. Meanwhile, PEMFCs have the slow rate of oxygen reduction under acidic conditions.

As an alternative to PEMDMFC, AEMDMFC have received great interest in recent years due to the following advantages: (i) a high pH value will provide enhancement in the electrode reaction kinetics,[3–6] (ii) AEMDMFC can operate with platinum free catalyst and greatly reduce the cost of the device,[7–9] (iii) new routes are available for addressing water management, and (iv) the electro osmotic drag of water from the air cathode to the fuel anode will lower fuel crossover.[10] Despite these benefits, the AEMDMFC suffers from the low diffusion coefficient of hydroxide ions. A membrane with high ionic conductivity may be obtained by the formation of nanochannels that facilitate ion transport or improve its ion exchange capacity.

There are various polymeric materials that can be used in AEMs, such as polyolefin,[11–13] poly(ether ketone),[14] polysulfone[15,16] and so on. The AEMs can be obtained by further chloromethylation, quaternization and alkalization. And the ammonium groups, phosphonium groups and sulfonium groups are always chosen for the solid polymer electrolyte.[17–20] Among the different species of exchange groups, ammonium groups are thought to have a higher thermal and chemical stability compared to other groups.

Addition-type polynorbornene (PNB) is a kind of suitable polymer material for DMFC with high thermal stability, good mechanical properties, excellent dielectric properties, low methanol permeability, as well as good chemical stability.[21–23] We have applied PNB to PEMFC in our previous studies.[24–28] A high ionic conductivity can be improved by increasing the amount of functional groups in the membrane. An effective strategy that we herein present is to introduce the functional

[a]School of Materials Science and Engineering, Nanchang University, 999 Xuefu Avenue, Nanchang 330031, China. E-mail: hexiaohui@ncu.edu.cn
[b]Jiangxi Provincial Key Laboratory of New Energy Chemistry, Nanchang University, 999 Xuefu Avenue, Nanchang 330031, China
[c]School of Civil Engineering and Architecture, Nanchang University, 999 Xuefu Avenue, Nanchang 330031, China

group onto the polymer structure, and to avoid attacking the β-hydrogen of the ammonium from the hydroxyl ions that leading to the degradation or loss of the mechanical properties of the membrane. Meanwhile, we design the molecular structure with nanophase separation which can form nanochannels between a hydrophobic matrix and hydrophilic side groups on the basis of Nafion's high conductivity with the similar structure.

In this study, we choose PNB as an organic polymer matrix to get high thermal stability, good dimensional stability and high ionic conductivity. Initial series of anion-conductive and durable quaternary ammonium functional addition-type norbornene copolymer (Q_{Cn}P(BN/PhBN), n = 1, 6, 10, 12) with different alkyl side chains length comb-shaped structures or different contents of 2-(4-phenyl-butoxymethy-lene)-5-norbornene (PhBN) (22–77%) are innovatively designed and prepared by using nickel catalyst in a vinyl-addition polymerization fashion. An important consequence is that the introduction of different long alkyl side chains pendant to the quaternary ammonium cation and the formation of comb-shaped structures while choosing PNB as polymer main chain, which can effectively build hydrophilic–hydrophobic separation, and thus enhance the ionic conductivities of these materials by forming the nanochannels. The obtained AEMs performances application in direct methanol fuel cell can be controllable by tuning the content of PhBN or adding different long alkyl side chains pendant to the nitrogen-centered cation.

2 Experimental

2.1 Materials

Toluene is refluxed and distilled from sodium and benzophenone under dry nitrogen, trimethylamine aqueous solution (30 wt%), tin(IV) chloride, chloromethyl methyl ether (CMME), phosphorus tribromide are obtained from Sigma-Aldrich Co. Sodium hydroxide, trichloromethane, and 5-norbornene-2-methanol are purchased from Puyang Huicheng chemical Co., Ltd, tetrahydrofuran (THF) is purchased from Tianjin Damao Chemical Reagent Factory of China, and chloroform-d is obtained from Aldrich Chemical. All chemicals are used as received, unless otherwise be specified. The catalyst, bis(β-ketonaphthylamino) nickel(II), is synthesized according to the method reported in our previous article.[29]

2.2 Addition polymerization

2.2.1 Synthesis of 2-butoxymethylene norbornene (BN). The monomer BN is synthesized by using a procedure reported by Liu *et al.*[24]

2.2.2 Synthesis of 2-butoxymethylene norbornene (PhBN). 4-Pheny-1-bromide-butane (M2) is synthesized by using a procedure reported by Hayward *et al.* with minor modifications.[30] 4-Phenylbutanol (M1) (5.0 g, 3.33×10^{-2} mol) in dry methylene chloride (100 mL) is added to a 250 mL flask, and sealed under a nitrogen atmosphere. The flask is placed in an ice water bath, and the mixture is stirred for 20 min. Phosphorus tribromide (3.16 mL, 3.33×10^{-2} mol) is added dropwise to the solution over a 15 min period. The reaction is running at room temperature for 8 hours, and then quenched with a 10% sodium bicarbonate solution. The organic solution is passed through a plug of Celite, rinsed with water, and dried over magnesium sulfate. The solution is filtered and dried by using rotary evaporation to yield the crude product. The crude product is further eluted over silica gel with petroleum ether, and the first of two UV active spots that seen by TLC are collected, and dried to obtain the product as a light yellow liquid (5.4 g, 77% yield). ^{1}H NMR ($CDCl_3$, δ, ppm): 7.26–7.15 (m, 5H, C_6H_5–), 2.6 (t, 2H, C_6H_5–CH_2–), 3.37 (t, 2H, –CH_2-Br), 1.87–1.72 (m, 4H, –CH_2–CH_2–).

The PhBN is synthesized by using the same route as that of BN synthesis, and the product is a yellow liquid. ^{1}H NMR ($CDCl_3$, δ, ppm): 7.26–7.15 (m, 5H, C_6H_5), 6.12–6.05 (m, 2H, –CH=CH–), 3.4 (t, 2H, norbornene-CH_2–O–), 3.27 (t, 2H, O–CH_2–C_3H_6–), 2.6 (t, 2H, C_6H_5–CH_2–), 2.76–0.84 (m, 6H, norbornene-6H), 1.68–1.1 (m, 4H, –CH_2–CH_2–).

2.2.3 Synthesis of P(BN/PhBN). Copolymerization of BN and PhBN (molar ratio = 9 : 1 or 7 : 3 or 5 : 5) is carried out by using a homogeneous catalyst that combination of bis(β-ketonaphthylamino) nickel(II) and $B(C_6F_5)_3$ in a round-bottom flask with a magnetic stirring bar and sufficiently purged with nitrogen. The appropriate $B(C_6F_5)_3$ solid, anhydrous toluene, BN, PhBN, and nickel(II) catalyst are added to the reactor sequentially. The copolymerization is conducted at 60 °C for 24 h and is terminated by adding HCl/EtOH (v/v = 1/9). The resulting P(BN/PhBN) copolymers {weight-average molecular weight (M_w) = 2.72×10^5, 1.94×10^5, 1.33×10^5 g mol^{-1}, respectively. Molecular weight distribution [MWD ≈ 2]} are separated off, washed with fresh methanol, and dried *in vacuo* at 40 °C until the weight remains constant. The total volume of the liquid phase is kept to be 10 mL.

2.3 Chloromethylation, quaternization, and membrane casting

Fresh trichloromethane (10 mL) is added to P(BN/PhBN) (0.2 g). Chloromethyl methyl ether (CMME) (0.15 mol) and $SnCl_4$ (0.01 mol) are then injected into the solution (**Caution**: CMME is carcinogenic and potentially harmful to human health). The reaction is allowed to continue for 5 h at 55 °C. Then the methanol is poured into the reaction mixture to get the crude chloromethylated polymer, named CP(BN/PhBN), and it is recovered by washing the precipitate several times with methanol.

The obtained chloromethylated copolymers CP(BN/PhBN) (0.20 g) are dissolved in THF (3 mL) and further quaternized by adding *N*,*N*-dimethylhexylamine (0.1 mol) to the copolymer at room temperature for 24 h. The solution is filtered with a 450 nm PTFE membrane filter and then cast onto a flat glass plate. The cast solution is dried at room temperature for 24 h to obtain a ductile membrane, named Q_{Cn}P(BN/PhBN). The chloride ions in the film are exchanged for hydroxide ions by soaking in 0.1 M NaOH for about 48 h. After washing several times with water, and the Q_{Cn}P(BN/PhBN) membranes in hydroxide form are achieved.

2.4 Characterization

2.4.1 ^{1}H NMR spectra. The chemical structures of the synthesized monomers and polymers are confirmed by analyzing the ^{1}H NMR and recorded on A Bruker AvanceIII 600 spectrometer. Chloroform-d is used as the NMR solvent. The ion exchange capacity (IEC) and degree of chloromethylation (DC) are determined from the respective ^{1}H NMR spectra.

2.4.2 GPC. The gel permeation chromatography (GPC) is conducted with a Breeze Waters system equipped with a Rheodyne injector, a 1515 Isocratic pump, and a Waters 2414 differential refractometer by using polystyrenes as the standard and tetrahydrofuran (THF) as the eluent at a flow rate of 1.0 mL min^{-1} and 40 °C through a Styragel column set, and the M_w is ranging from 10^2 to 10^6.

2.4.3 Thermal analysis and mechanical properties. Thermal degradation and stability of the membranes are investigated by using a thermo-gravimetric analyzer (TGA) (Perkin-Elmer instrument TGA 7) under a nitrogen atmosphere at a heating rate of 20 °C min^{-1} from room temperature to 800 °C. The mechanical properties are measured on a CMT8502 Machine model GD203A (ShenZhen Sans Testing Machine, China) at a speed of 5 mm min^{-1}.

2.4.4 Contact angle measurements and microscopic characterizations. Contact angle measurements are performed on surfaces of every prepared membranes with drops of water by using Powereach JC2000A Interface Tension/Contact Angle Measure Equipments to study the hydrophilicity. Samples are spin coated onto the quartz glass substrates at a spin speed of 2000 rpm for 40 s and then thermally annealed at 60 °C for 5 min.

The surface morphology of the dried membranes are studied by a JEOL JEM-2100F transmission electron microscope (TEM). Samples for transmission electron microscopy (TEM) are prepared as follows:[31] membranes are stained by soaking in 1 mol L^{-1} sodium tungstate solution overnight, then washed several times with water and dried under vacuum at room temperature. The samples are dissolved in THF and coated on copper grids.

The surface and cross section morphology of the membranes are investigated by scanning electron microscope (SEM) and Environmental Scanning Electron Microscope (ESEM, FEI Quanta 200). All samples are soaked in the liquid nitrogen and fractured, followed by the sputtering of a thin layer of gold.

2.4.5 Dimensional stability and uptake of water. The swelling ratio of the OH^- form membranes in plane (SR_p) and in thickness (SR_t) direction are measured by the following equations:

$$SR_p = \frac{l_{wet} - l_{dry}}{l_{dry}} \quad (1)$$

$$SR_t = \frac{t_{wet} - t_{dry}}{t_{dry}} \quad (2)$$

where $l_{wet} = \sqrt{a_{wet} b_{wet}}$ and $l_{dry} = \sqrt{a_{dry} b_{dry}}$ are the average length of wet and dry membrane samples, respectively, in which, a and b are the lengths and widths of wet and dry membrane samples, respectively. t_{wet} and t_{dry} are the thickness of wet and dry membranes, respectively.

For the measurement of water uptake, the membranes are immersed in deionized water for 48 h under different temperature conditions, and the wet membranes are weighted after the surface being wiped with tissue paper. These wet membranes are dried at a set temperature of 60 °C until constant dry weight is obtained. The uptake of water (η_w) is calculated by using the following equation:

$$\eta_w(\%) = \frac{m_{wet} - m_{dry}}{m_{dry}} \times 100\% \quad (3)$$

where m_{dry} and m_{wet} are the weight of dry and wet membrane samples, respectively. The uptake of water is the average of the measurement by three times.

2.4.6 Ion-exchange capacity (IEC). The ion-exchange capacity is defined as the ratio between the number of exchangeable ionic groups and the weight of the dry membrane. The IECs of membranes are determined by the back titration method. Briefly, the dried OH^- form membranes are immersed in 50 mL 0.01 M HCl aqueous solutions for 24 h, followed by back titration of 0.01 M NaOH solution as the indicator. The 30 mL 0.01 M HCl solution is used as the blank sample for the contrast experiment. The measured IEC (mmol g^{-1}) of the membrane is calculated as follows:

$$IEC = \frac{C_{HCl} V_{HCl} - C_{NaOH} V_{NaOH}}{M} \quad (4)$$

where V_{NaOH} and V_{HCl} is the consumed volume (mL) of the NaOH solution and HCl solution, respectively. C_{NaOH} and C_{HCl} are the concentration of NaOH solution and HCl solution (mol L^{-1}), M is the mass of dry membrane.

2.4.7 Membrane conductivity measurements. The ionic conductivity (δ) of the membrane is evaluated at different temperatures (30–90 °C) by three-electrode electrochemical impedance spectra method, using a CHI660 electrochemical workstation (CH Instruments). The sample is sandwiched between two PTFE gaskets in a PTFE diffusion cell that composed of two symmetrical chambers. The cell is filled with the electrolyte composed of 1 M NaOH solution.

The two platinum wires are used as the working electrode and counter electrode, as well as a Ag/AgCl electrode functionalized as the reference electrode that introduced into the electrolyte solution. The impedance spectra are recorded with the help of ZPlot/ZView software under an ac perturbation signal of 10 mV over the frequency range of 1–10^5 Hz. The electric resistance of the system (without membrane divided) is measured as R_1, and the electric resistance of the system (with membrane divided) is measured as R_2. The difference value ($R_2 - R_1$) is the testing value of the anion exchange membrane resistance (R). The ionic conductivity (δ) of the membrane is calculated from the following equation:

$$\delta = l/(RA) \quad (5)$$

where δ, l, R and A are the ionic conductivity, thickness of membranes, the resistance of the membrane, and the cross-sectional area of the membrane, respectively.

2.4.8 Methanol permeability measurements. An organic glass diffusion cell is used to obtain the methanol permeability of the membrane. The diffusion cell is composed of two membrane sample. One chamber of the cell (V_1) is filled with 5 M (C_1) methanol solution in distilled water. The other chamber (V_2) is filled with water. A sample is clamped between the two chambers. Methanol permeates across the membrane by the concentration difference between the two chambers, which can prompt methanol into distilled water. Then we collect the solution from distilled water at every same time, the concentration of it is defined C_2. The methanol concentration in the receiving chamber as a function of time is given by the equation:

$$C_2(t) = [ADKC_1(t_1 - t_0)/(V_1 l)] \quad (6)$$

where A (cm^2) is the membrane area, l (cm) is the membrane thickness, D is the methanol diffusivity, and K is the partition coefficient between the membrane and the adjacent solution. The product DK means the membrane permeability (P):

$$P = (C_2(t)V_1 l)/[AC_1(t_1 - t_0)] \quad (7)$$

C_2 is measured several times during the permeation experiment and the methanol permeability is obtained from the slope of the straight line. The methanol concentration is measured by using a gas chromatography of Agilent 7890A GC system equipped with a FID detector.

2.4.9 Single-cell performance tests. The catalyst solution is prepared by mixing 40% Pt/C (Hesen) with a solution of 5 wt% Nafion (DuPont) and isopropanol, and then sonicated for 5 h to get a homogeneous solution. The catalyst solution is sprayed onto the carbon paper to obtain a catalyst layer with a Pt loading of 0.5 mg cm^{-2} for both anode and cathode.

MEA (membrane electrode assembly) is fabricated by hot-pressing the alkalized Q_{C12}P(BN/PhBN)-77 AEM along with the anode and cathode catalyst layer for 5 min under pressure of 6 MPa at 60 °C. The MEA is evaluated in a single fuel cell with an active area of 4 cm^2 in methanol/air. Methanol and air are supplied to enter the anode and cathode channels at a flow rate of 3 mL min^{-1} and 300 mL min^{-1}, respectively. Polarization curves are obtained by using a commercial fuel cell evaluation system (Arbin BT 2000) at 80 °C.

3 Results and discussion

3.1 Synthesis and characterization of comb-shaped copolymers

A series of copolymers P(BN/PhBN), chloromethylated copolymers CP(BN/PhBN), and quaternized copolymers Q_{Cn}P(BN/PhBN) are synthesized as shown in Scheme 1.

The structures of P(BN/PhBN) and CP(BN/PhBN) are characterized by ^{1}H NMR spectroscopy (Fig. 1), it proves that the polymers are vinyl-addition type by the resonance absence of the proton hydrogen connected to the double bond at 6.12–6.05 ppm. The peak at 3.4 ppm can be assigned to the hydrogen corresponding to a/b, the peak at 2.6 ppm can be assigned to the hydrogen corresponding to c (Fig. 1a).

The chloromethyl group is introduced to P(BN/PhBN) (Fig. 1b), and chloromethylated protons appear at 4.5 ppm. The contents of PhBN in copolymers can be carefully controlled by adjusting the monomer feed ratios (BN/PhBN = 9/1, 7/3, 5/5). And it can be calculated to be (a) 22%, (b) 40%, and (c) 77% by the following equation.

$$\frac{A}{B} = \frac{2x}{4x + 4y}$$

A is the integral area of peak a/b, B is the c, x was set as the contents of PhBN, y is set as the contents of BN, and $x + y = 1$.

At the same time, the degree of chloromethylation can be calculated by the same method with the area ratio of ^{1}H NMR peaks k and m, which are 87%, 71%, and 64% and shown in Table 4.

The P(BN/PhBN) copolymers are obtained by using Ni(II)/$B(C_6F_5)_3$ catalytic system and characterized by GPC (as shown in Fig. 2). The M_w data of the obtained copolymers are all up to 10^5, and the WMD data are all relative narrow (WMD = 1.75–2.49). The relative narrow MWD and appearing as a single modal in the GPC chromatogram indicate that copolymerization occurs at the single active site, and the products are the true copolymers instead of blends of homopolymers. The polymerization results are presented in Table 1.

3.2 Membrane appearance and surface hydrophilicity

All the alkaline membranes with a thickness around 200 nm are homogeneous, flexible, and yellow. The membranes and their corresponding solution before alkalization are presented in Fig. 3.

Values of measured contact angles are shown in Fig. 4. It is assumed that the polynorbornene main chain showed strong hydrophobicity which restricted the hydrophilicity of the polymers. The grafted side chain could effectively improve the hydrophilicity of the polynorbornene main chain, which could be illuminated by the relatively small contact angles of all the membranes. Q_{C12}P(BN/PhBN)-77 membrane has the best hydrophilicity, indicating that the smaller contact angle can be observed in membranes with longer side chain or lager contents of hydrophilicity PhBN segment.

3.3 Microscopic characterizations

Furthermore, the microscopic characterizations of the alkaline membranes are studied by TEM and SEM. All of the alkaline membranes show no cracks and holes on the membrane surface indicate the dense nature of the membrane (Fig. 5a and c). The even-distributed nanosized spot like structure on the membrane surface indicate that the micro phase separation (Fig. 5b) is formed between the hydrophobic main chain and the hydrophilic side chain structure of polymer. And the white particle is called the ion domain which is beneficial to the formation of ion transport channel[32,33] and can improve the ionic conductivity. The micro-morphology stemmed from the comb-shaped copolymer is further confirmed by TEM

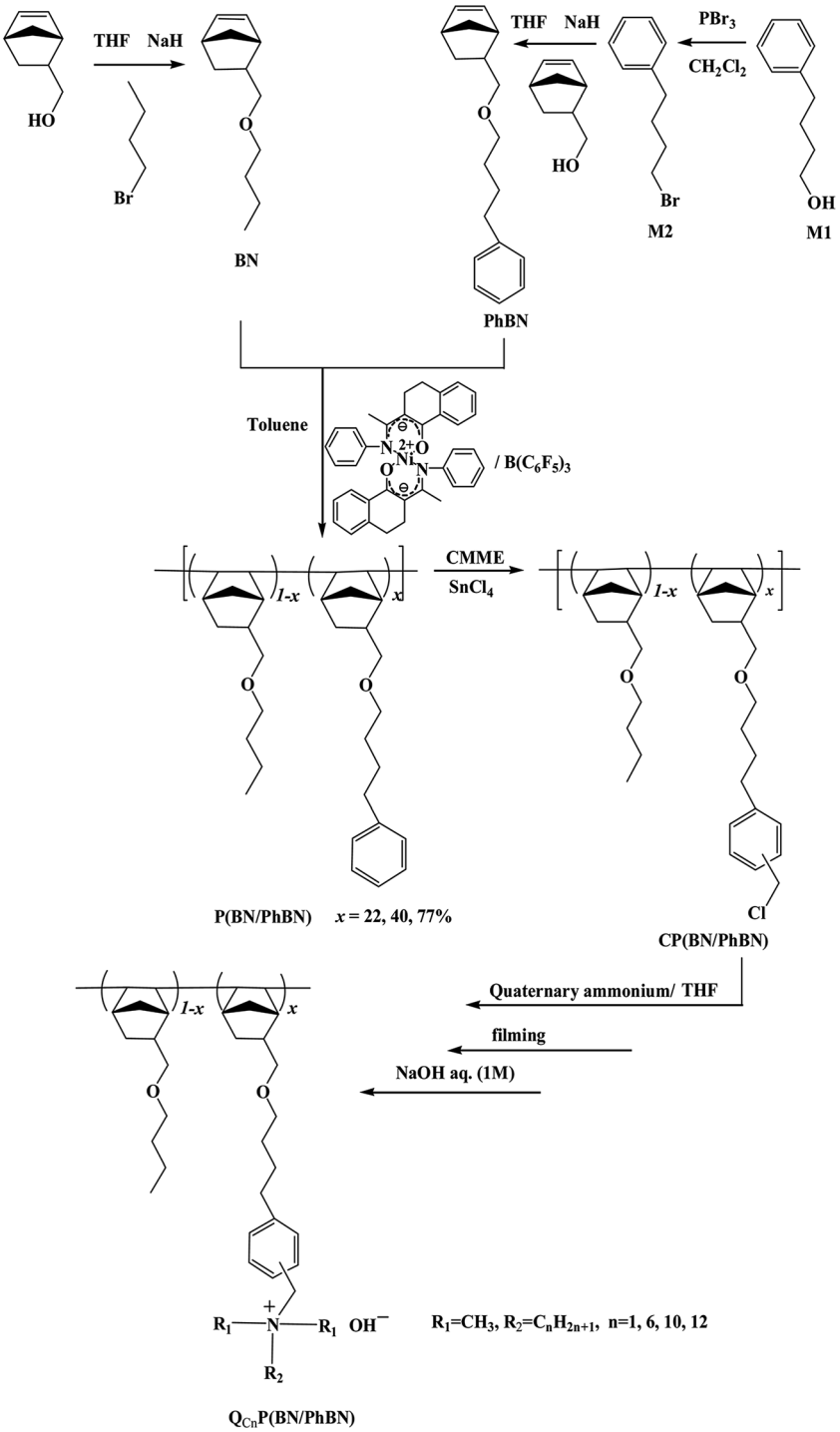

Scheme 1 Synthesis of comb-shaped P(BN/PhBN), CP(BN/PhBN), and Q_{Cn}P(BN/PhBN) copolymers.

technique. The TEM images of alkalized Q_{C6}P(BN/PhBN)-22 provide a direct evidence of biphasic morphology for the polymer membranes and exhibit a clear hydrophilic–hydrophobic microphase separation with wormlike and interconnect hydrophilic network nanochannels (Fig. 5d). This unique micromorphology supports sufficient hydroxide conducting through uniformly distributed well-connected ion pathways. The light regions are corresponded to the hydrophobic domains of the P(BN/NB) main chains while the dark regions are corresponded to the hydrophilic PhBN side chains.

3.4 Thermal stability and mechanical properties

Fig. 6 shows the TGA data for the comb-shaped copolymers Q_{Cn}P(BN/PhBN) (in OH^- form). From the diagram we can know, its decomposition can be divided into four parts in the TGA

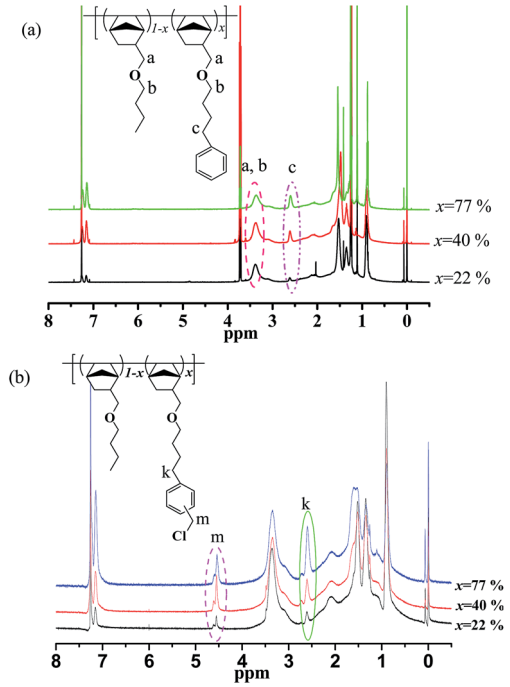

Fig. 1 ^{1}H NMR spectra of copolymers (in $CDCl_3$): (a) P(BN/PhBN); (b) chloromethylation of P(BN/PhBN).

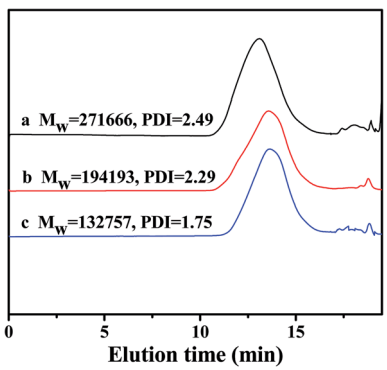

Fig. 2 The GPC curves of BN/PhBN copolymers with PhBN molar ratios: (a) 22%, (b) 40%, (c) 77% obtained by bis(β-ketonaphthylamino) Ni(II)/$B(C_6F_5)_3$ system.

curve for QP(BN/PhBN). Firstly, a slight loss between 50 and 150 °C corresponding to the evaporation of absorbed water is observed due to strong hydrophilicity of the quaternary ammonium groups attracting water from the atmosphere. Secondly, the elimination of quaternary ammonium groups occurs at 160 °C, and the loss percentage increases with the graft ratio increasing. Thirdly, the mass loss commences at 280–420 °C that is accredited to the decomposition of the side chains of copolymers.[31] Fourthly, the weight loss at around 430 °C is related to the degradation of the polymer backbone.[26] Based on these observations, we can conclude that the thermal stability of this membrane is able to satisfy the requirement of application in direct methanol fuel cell.

The tensile curves of the copolymer films with different PhBN content and different alkyl side chains are shown in Fig. 7, and the mechanical properties are presented in Table 2. The film of copolymer that contains 22.0% PhBN shows the best mechanical properties, and the tensile strength is about 6.1–7.9 MPa and the elastic modulus is 300.1–488.5 MPa, the toughness and strength are enough to meet the application requirements in fuel cells.

3.5 Water uptake and dimensional swelling

For fuel cell application, water uptake (WU) is of particular importance in evaluating the performance of the AEMs. Excess water adsorption will lead to deterioration in the thermal, mechanical, dimensional, chemical stabilities and ionic concentration. Table 3 shows the water uptake data of the copolymer membranes evaluated at 25 °C and 60 °C. Generally, higher IEC values can give higher water uptake because both properties are strongly related to the amount of quaternary ammonium group (Tables 3 and 4). Q_{C12}P(BN/PhBN)-77 membranes with maximum chloromethyl grafting ratio exhibits 16.3% of water uptake at 25 °C, which is lower than Nafion 117.

The dimensional stability of these membranes, which is one of the crucial properties of AEMs for their application in fuel cells, is evaluated by the water swelling ratio. A low in-plane swelling is particularly expected to inhibit the deamination of catalyst layer caused by dimensional mismatch. Herein, the in-plane swelling ratio is low (the highest value is 4.21% at 60 °C), suggesting that the obtained membranes can meet the requirements for dimensional stability in fuel cells application.

3.6 IEC, ionic conductivity and methanol permeability

The ion-exchange capacity (IEC) data of AEMs are calculated to be from 0.91 to 1.81 mol g^{-1} by the integral ratios, which is in good agreement with the calculated values from the copolymer compositions and the degree of chloromethylation. And these

Table 1 The results of vinyl-addition type copolymerizations with different monomer feed ratios[a]

Sample	BN/PhBN (mol mol^{-1})	Mol% of PhBN in copolymers	Activity ($g_{polymer}$ (mol_{Ni} h)$^{-1}$)	Yield (%)	M_w ($\times 10^5$)	PDI
P(BN/PhBN)-22	9/1	22	1.2×10^4	63.7	2.72	2.49
P(BN/PhBN)-40	7/3	40	1.0×10^4	47.7	1.94	2.29
P(BN/PhBN)-77	5/5	77	0.6×10^4	25.6	1.33	1.75

[a] Conditions: (1) $n_{[Cat.]}$ is 5.0×10^{-6} mol; (2) co-catalyst is $B(C_6F_5)_3$; (3) B/Cat./monomer is 20/1/2000 (molar ratio); (4) polymerization temperature sets as 60 °C; (5) solvent: toluene; (6) V_p = 10 mL; (7) polymerization time: 24 h.

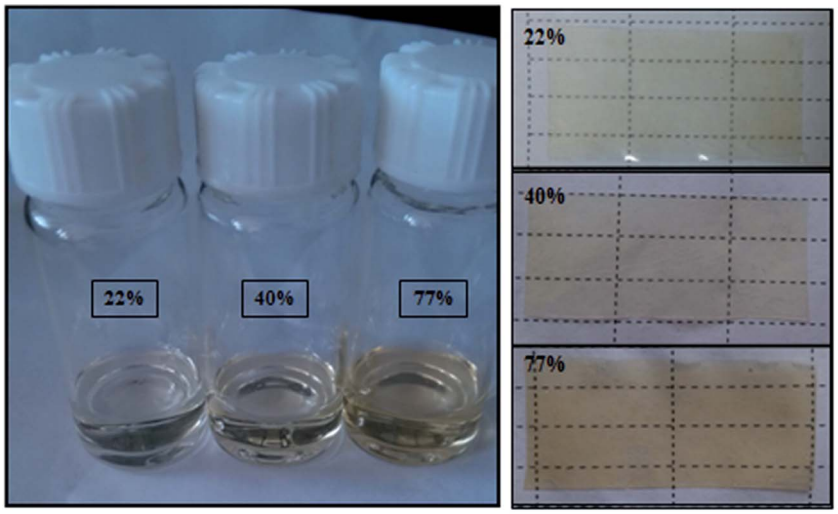

Fig. 3 The photographs of $Q_{C12}P(BN/PhBN)$ with different degree of chloromethylation: (1) $Q_{C12}P(BN/PhBN)$-22; (2) $Q_{C12}P(BN/PhBN)$-40; (3) $Q_{C12}P(BN/PhBN)$-77.

IEC values calculated from ^1H NMR are similar to the values determined from titration, further suggesting that quaternization of the chloromethyl groups occurs successfully, and has no side effects (Table 4). $Q_{Cn}P(BN/PhBN)$ with maximum grafting ratio has IEC of 1.81×10^{-3} mol g^{-1}, which is relatively higher than that of Nafion 117 might be due to higher quaternary ammonium group.

It is well known that the IEC values directly depend on the content of quaternary ammonium group incorporated into the polymer and thus they are indicative of the actual ion exchange sites available for ionic conduction.[34] Ionic conductivity data for different composite membranes are also presented in Table 4. It can be seen that conductivity values increase with the PhBN content increasing in the membrane matrix. The $Q_{C12}P(BN/PhBN)$-77 show the highest ionic conductivity of 4.14×10^{-3} S cm^{-1}, lower than Nafion117 (9.56×10^{-2} S cm^{-1}),[35] which may be due to the lower water uptake. More quaternary ammonium groups that facilitate transporting hydroxide and moderate water retention ability resulting from the comb-shaped structure may be two of the reasons for the observed variations in ionic conductivity values. Combined with the moisture content data (Table 3) of this film, we discover that with the growth of the quaternary ammonium side chain, the water absorption of this polymer membranes is enhanced. It is noteworthy that ionic conductivity also increases. The above results indicate that the comb-polymer can build micro-phase separation, which can

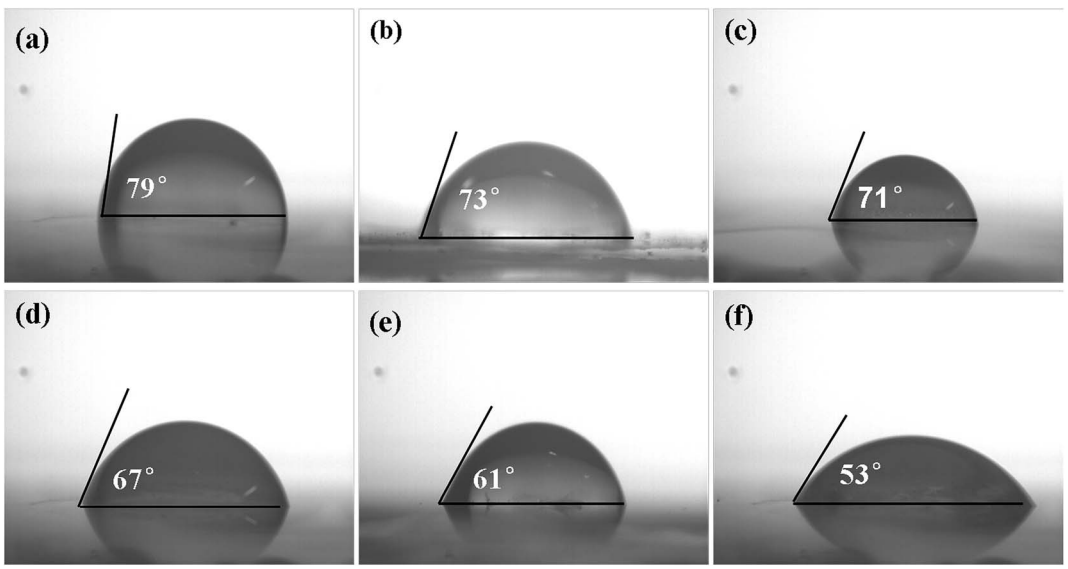

Fig. 4 Water contact angle images of alkalized (a) $Q_{C1}P(BN/PhBN)$-22; (b) $Q_{C6}P(BN/PhBN)$-22; (c) $Q_{C10}P(BN/PhBN)$-22; (d) $Q_{C12}P(BN/PhBN)$-22; (e) $Q_{C12}P(BN/PhBN)$-40; (f) $Q_{C12}P(BN/PhBN)$-77 membranes.

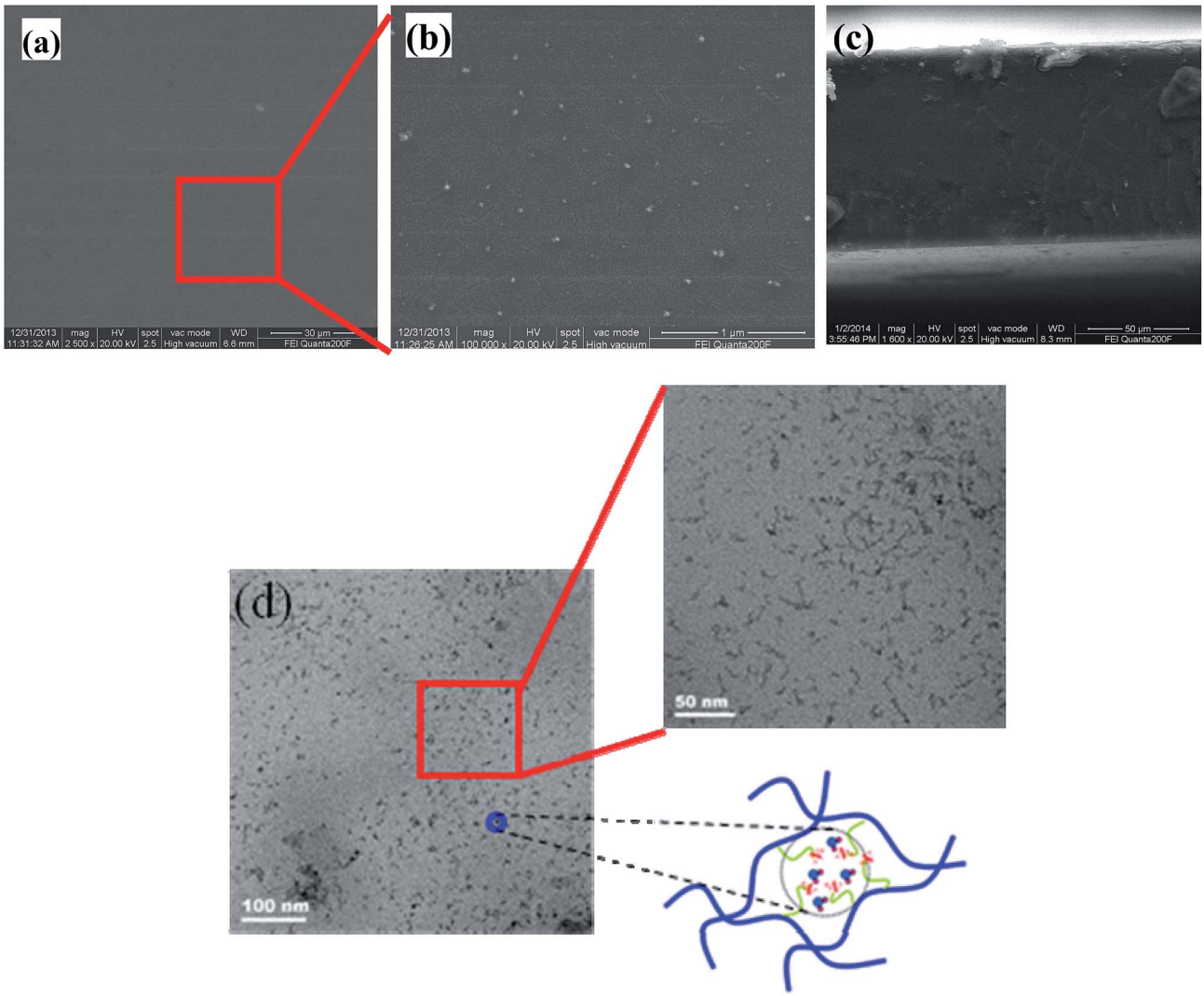

Fig. 5 The SEM and TEM images of alkalized Q_{C6}P(BN/PhBN)-22 membrane: (a) SEM surface (30 μm); (b) SEM surface (1 μm); (c) SEM cross-section (50 μm); (d) TEM image of the copolymer staining with tungstate ions.

efficiently adjust the transmission channel of OH^-, this theory has been confirmed in the study of proton exchange membrane.[36] The temperature-dependent conductivity measurements from 30 to 80 °C are conducted and shown in

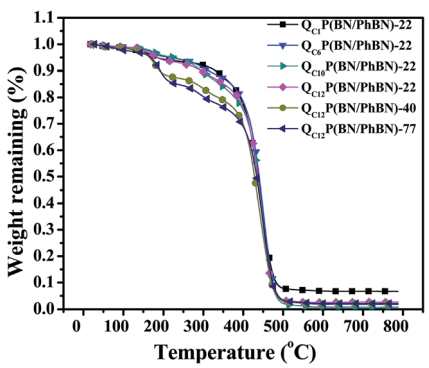

Fig. 6 TGA thermograms of the alkalized Q_{Cn}P(BN/PhBN) membranes recorded using a 20 °C min^{-1} heating rate under nitrogen atmosphere.

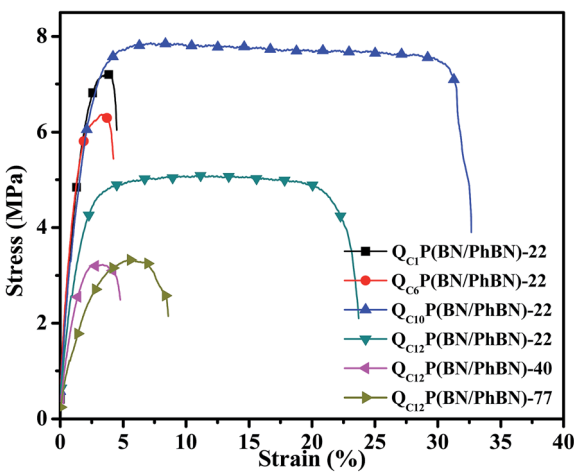

Fig. 7 The tensile curves of alkalized Q_{Cn}P(BN/PhBN) with different quaternary ammonium groups.

Table 2 The key mechanical properties of alkalized Q_{Cn}P(BN/PhBN) membranes

Sample	Tensile strength at break (MPa)	Elongation at break (%)	Elastic modulus (MPa)
Q_{C1}P(BN/PhBN)-22	7.2	4.5	450.2
Q_{C6}P(BN/PhBN)-22	6.4	4.2	488.5
Q_{C10}P(BN/PhBN)-22	7.9	32.7	393.1
Q_{C12}P(BN/PhBN)-22	5.1	23.7	300.1
Q_{C12}P(BN/PhBN)-40	3.2	4.8	206
Q_{C12}P(BN/PhBN)-77	3.3	8.6	159.2

Fig. 8. We observe the increase of conductivity with the operation temperature increasing. Delightfully, in contrast to the QP(BN/PhBN), ionic conductivity increased with increasing of the quaternary ammonium group into the polymer matrix and the test temperatures.

The relevant data of methanol permeability for all Q_{Cn}P(BN/PhBN) membranes are determined and presented in Table 4. Methanol permeability coefficients for these Q_{Cn}P(BN/PhBN)-22 membranes (1.99–2.01 $\times$ 10^{-7} cm^2 s^{-1}) are lower than one order of magnitude in comparison with Nafion117 (1.31 $\times$ 10^{-6} cm^2 s^{-1}).[37] It's known that the permeation of liquid molecules across polymer membrane happened *via* the diffusion mechanism, and the permeability of penetrate (methanol is one of the case) is the product of its solubility and diffusivity. On account of the narrow free void volume, the rigid structure of the addition-type polynorbornene main chain hindered the methanol to penetrate into the membranes. The methanol permeability of the membranes increased with the hydrophilic side chain, because of the hydrophilicity contributes to increasing water uptake and methanol permeability and thus causing broadening of the ion-conducting channels to some extent.

3.7 Chemical stability

Besides the excellent thermal stability, the long-term tolerance of Q_{Cn}P(BN/PhBN) membrane is also investigated in NaOH solutions (6 mol L^{-1}). The hydroxide conductivities of Q_{C1}P(BN/PhBN)-22, Q_{C12}P(BN/PhBN)-22 and Q_{C12}P(BN/PhBN)-77 membranes are plotted as a function of time in Fig. 9. In alkaline environments, the degradation of quaternary ammonium groups is usually derived from the strong nucleophilicity of the OH^- anions, which leading to displacement (SN_2) and Hofmann elimination reactions. After an initial period of decline behavior for 5 days, the conductivity values of the Q_{C1}P(BN/PhBN)-22 membrane is remained constant over longer immersion period. However, the conductivity values of the Q_{C12}P(BN/PhBN)-22 and Q_{C12}P(BN/PhBN)-77 decrease little as time goes on because of the β-H on the ammonium leading to Hofmann elimination reactions. These results demonstrate that the chemical stability of the comb-shaped membranes is excellent.

3.8 DMFC single cell performance

The alkalized Q_{C12}P(BN/PhBN)-77 is chosen as AEM for testing the single cell performance owing to the highest hydroxide ion

Table 3 Thickness, water uptake, in-plane swelling and in-thickness swelling of Q_{Cn}P(BN/PhBN) AEMs

Sample	Thickness (nm)	Water uptake (%)		In-plane swelling (%)		In-thickness swelling (%)	
		25 °C	60 °C	25 °C	60 °C	25 °C	60 °C
Q_{C1}P(BN/PhBN)-22	80	1.8	3.4	1.02	1.18	0.63	0.77
Q_{C6}P(BN/PhBN)-22	90	2.5	4.2	1.25	1.32	0.86	0.93
Q_{C10}P(BN/PhBN)-22	125	4.9	8.8	1.78	2.03	1.0	1.41
Q_{C12}P(BN/PhBN)-22	109	5.8	9.7	2.01	2.88	0.9	1.43
Q_{C12}P(BN/PhBN)-40	132	8.5	16.1	2.75	3.59	1.5	1.95
Q_{C12}P(BN/PhBN)-77	145	16.3	23.1	3.3	4.21	4.4	5.2

Table 4 DC, IEC, anion conductivity, methanol permeability of the Q_{Cn}P(BN/PhBN) AEM

Sample	DC (%)	IEC($\times 10^{-3}$ mol g^{-1})		Conductivity (80 °C) (10^{-3} S cm^{-1})	Methanol permeability[c] (10^{-7} cm^2 s^{-1})
		Calculated[a]	Titrated[b]		
Q_{C1}P(BN/PhBN)-22	87	0.91	0.85	1.32	2.01
Q_{C6}P(BN/PhBN)-22	87	0.91	0.90	1.63	1.99
Q_{C10}P(BN/PhBN)-22	87	0.91	0.89	2.05	2.01
Q_{C12}P(BN/PhBN)-22	87	0.91	0.93	2.23	2.00
Q_{C12}P(BN/PhBN)-40	71	1.18	1.14	3.53	4.01
Q_{C12}P(BN/PhBN)-77	64	1.81	1.83	4.14	20.40

[a] Calculated by the ^{1}H NMR spectrum Fig. 1b. [b] Calculated by the titrated method. [c] All data were tested at room temperature.

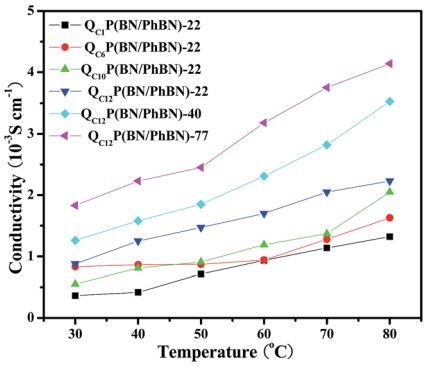

Fig. 8 Ionic conductivity of alkalized Q_{Cn}P(BN/PhBN) membrane as a function of temperature.

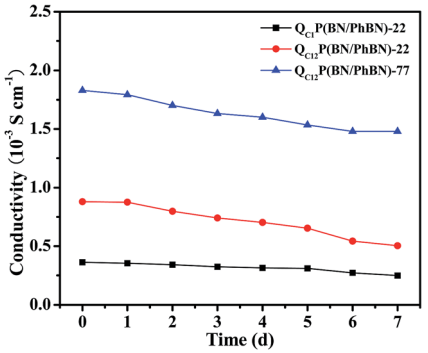

Fig. 9 The change trend in conductivity of alkalized Q_{Cn}P(BN/PhBN) after immersion in 6 M NaOH solution at room temperature.

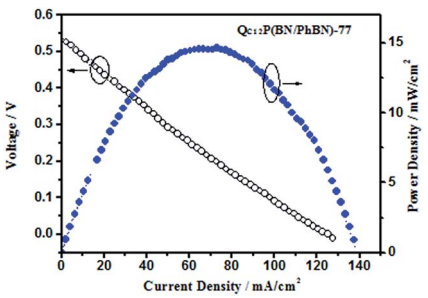

Fig. 10 DMFC single cell performance curves of the alkalized Q_{C12}P(BN/PhBN)-77 membrane at 80 °C.

conductivity, the performance of DMFC is evaluated at 80 °C with methanol/air in a alkaline media. As shown in Fig. 10, the open circuit voltage (OVC) of the fuel cell is 0.54 V, and the cell delivers a power density of 14 mW cm^{-2} and a current density of 66 mW cm^{-2}. It is evident that the performance value is lower than other studied polymer AEMs,[38,39] the reason is probably due to the lower ion conductivity and poor contact between the membrane and the catalyst layer.

4 Conclusions

A series of anion-conductive and durable polymer electrolyte AEMs are achieved, successfully. The obtained AEMs have excellent dimensional stability with swelling degree in plane between 0.9–3.3%, as well as high ion exchange capacity up to 1.83 mmol g^{-1}. The thermal stability and mechanical properties of the membranes are also excellent. When the membranes are soaked into NaOH solution (6 M), their ionic conductivity hardly decayed after a week. Meanwhile, the conductivity increase with the operation temperature or IEC, and up to 4.14×10^{-3} S cm^{-1} at 80 °C. Moreover, methanol permeability of these membranes is in the range of $1.97–20.4 \times 10^{-7}$ cm^2 s^{-1}, which is lower than that of Nafion®. The alkalized Q_{C12}P(BN/PhBN)-77 AEM Performance of methanol/air fuel cell show a maximum open circuit voltage (OVC) of 0.54 V and current density of 66 mW cm^{-2} at 80 °C, respectively. Further work will focus on enhancing its ion conductivity and cell performance to satisfy the AEMs requirement as potential application in DMFC.

Acknowledgements

This work is supported by the National Natural Science Foundation of China (51463014 and 21164006).

References

1 Y. J. Wang, J. L. Qiao, R. Baker and J. J. Zhang, *Chem. Soc. Rev.*, 2013, **42**, 5768–5787.
2 H. C. Tao, X. N. Sun and Y. Xiong, *RSC Adv.*, 2015, **5**, 4659–4663.
3 A. V. Tripković, K. D. Popović, B. N. Grgur, B. Blizanac, P. N. Ross and N. M. Marković, *Electrochim. Acta*, 2002, **47**, 3707–3714.
4 M. R. Hibbs, *J. Polym. Sci., Part B: Polym. Phys.*, 2013, **51**, 1736–1742.
5 E. Kjeang, N. Djilali and D. Sinton, *J. Power Sources*, 2009, **186**, 353–369.
6 T. P. Pandey, A. M. Maes, H. N. Sarode, B. D. Peters and A. M. Herring, *Phys. Chem. Chem. Phys.*, 2015, **17**, 4367–4378.
7 L. Zeng, T. S. Zhao and L. An, *J. Mater. Chem. A*, 2015, **3**, 1410–1416.
8 J. John, K. M. Hugar, J. Rivera-Meléndez, H. A. Kostalik IV, E. D. Rus, H. Wang, G. W. Coates and H. D. Abruna, *J. Am. Chem. Soc.*, 2014, **136**, 5309–5322.
9 F. P. Hu, F. Ding, S. O. Song and P. K. Shen, *J. Power Sources*, 2006, **163**, 415–419.
10 R. Mosdale and S. Srinivasan, *Electrochim. Acta*, 1995, **40**, 413–421.
11 S. Maurya, S. H. Shin, K. W. Sung and S. H. Moon, *J. Power Sources*, 2014, **255**, 325–334.
12 T. A. Sherazi, J. Yong Sohn, Y. Moo Lee and M. D. Guiver, *J. Membr. Sci.*, 2013, **441**, 148–157.
13 W. T Lu, Z. G. Shao, G. Zhang, Y. Zhao and B. L Yi, *J. Power Sources*, 2014, **248**, 905–914.
14 J. H. Pang, S. N. Feng, Y. Y. Yu, H. B. Zhang and Z. H. Jiang, *Polym. Chem.*, 2014, **5**, 1477–1486.
15 L. D. Liu, C. Y. Tong, Y. He, Y. X. Zhao and C. L. Lü, *J. Membr. Sci.*, 2015, **487**, 99–108.
16 X. F. Liao, L. Ren, D. Z. Chen, X. H. Liu and H. W. Zhang, *J. Power Sources*, 2015, **286**, 258–263.

17 K. J. Noonan, K. M. Hugar, H. A. t. Kostalik, E. B. Lobkovsky, H. D. Abruna and G. W. Coates, *J. Am. Chem. Soc.*, 2012, **134**, 18161–18164.
18 B. Qiu, B. Lin, L. Qiu and F. Yan, *J. Mater. Chem.*, 2012, **22**, 1040–1045.
19 J. Choi, Y. J. Byun, S. Y. Lee, J. H. Jang, D. Henkensmeier, S. J. Yoo, S. A. Hong, H. J. Kim, Y. E. Sung and J. S. Park, *Int. J. Hydrogen Energy*, 2014, **39**, 21223–21230.
20 J. Wang, Z. Zhao, F. Gong, S. Li and S. Zhang, *Macromolecules*, 2009, **42**, 8711–8717.
21 S. Martînez-Arranz, A. C. Albéniz and P. Espinet, *Macromolecules*, 2010, **43**, 7482–7487.
22 J. H. Park, T. W. Koh, J. Chung, S. H. Park, M. Eo, Y. Do, S. Yoo and M. H. Lee, *Macromolecules*, 2013, **46**, 674–682.
23 D. P. Song, H. L. Mu, X. C. Shi, Y. G. Li and Y. S. Li, *J. Polym. Sci., Part A: Polym. Chem.*, 2012, **50**, 562–570.
24 S. F. Liu, Y. W. Chen, X. H. He, L. Chen and W. H. Zhou, *J. Appl. Polym. Sci.*, 2011, **121**, 1166–1175.
25 X. F. Wang, J. Q. Hu, T. Hu, Y. Zhang, Y. W. Chen, W. F. Zhou, S. Q. Xiao and X. H. He, *J. Appl. Polym. Sci.*, 2012, **123**, 3225–3233.
26 X. H. He, M. P. Hu, Y. W. Chen and D. F. Chen, *J. Power Sources*, 2013, **242**, 725–731.
27 H. L. Yao, X. H. He, L. Chen, Y. W. Chen and D. F. Chen, *J. Appl. Polym. Sci.*, 2013, **128**, 3540–3547.
28 X. H. He, Y. Zheng, H. L. Yao, Y. W. Chen and D. F. Chen, *Fuel Cells*, 2014, **1**, 26–34.
29 K. T. Wang, Y. W. Chen, X. H. He, Y. M. Liu and W. H Zhou, *J. Polym. Sci., Part A: Polym. Chem.*, 2011, **49**, 3304–3313.
30 E. Lee, B. Hammer, J. K. Kim, Z. Page, T. Emrick and R. C. Hayward, *J. Am. Chem. Soc.*, 2011, **133**, 10390–10393.
31 J. Ran, L. Wu and T. W. Xu, *Polym. Chem.*, 2013, **4**, 4612–4620.
32 Suryani and Y. L. Liu, *J. Membr. Sci.*, 2009, **332**, 121–128.
33 E. B. Cho, D. X. Luu and D. Kim, *J. Membr. Sci.*, 2010, **351**, 58–64.
34 R. Patel, S. J. Im and Y. T. Ko, *J. Ind. Eng. Chem.*, 2009, **15**, 299–303.
35 B. P. Tripathi and V. K. Shahi, *J. Phys. Chem. B*, 2008, **112**, 15678–15690.
36 Y. A. Elabd and M. A. Hickner, *Macromolecules*, 2010, **44**, 1–11.
37 B. P. Tripathi and V. K. Shahi, *ACS Appl. Mater. Interfaces*, 2009, **1**, 1002–1012.
38 J. Zhang, J. L. Qiao, G. P. Jiang, L. L. Liu and Y. Y. Liu, *J. Power Sources*, 2013, **240**, 359–367.
39 K. Tran, T. Q. Nguyen, A. M. Bartrom, A. Sadiki and J. L. Haan, *Fuel Cells*, 2014, **14**, 834–841.